# Helium plasmas operation domain studies on the GOLEM tokamak

**Vojtech Svoboda[1], Jan Stockel[1,2], Alexander Melnikov[3,4], Nikita Sergeev[3,4], Alexey Drozd[3,4], Daniela Kropachkova[1], Martina Lauerova[1], Vladimir Kulagin[3,4], Stanislav Ganin[3,4], Ivan Kudashev[3,4]**

[1]*Faculty of Nuclear Sciences and Physical Engineering Prague, Czech Republic*

[2]*Institute of Plasma Physics, AS CR, Za Slovankou 3, 182 00 Prague, Czech Republic*

[3]*National Research Nuclear University "MEPhI", Moscow, Russian Federation*

[4]*National Research center "Kurchatov Institute", Moscow, Russian Federation*

**E-mail**: vojtech.svoboda@fjfi.cvut.cz

**Abstract**

The issue of helium plasma confinement in modern tokamaks remains an important area of research. This work is dedicated to the study of helium plasma initiation and its control in a small-scale machine GOLEM. The comparison between helium and hydrogen plasma discharges are done. Main plasma parameters evolution for both types of gas is presented here during start-up and burn-through phase of the discharge. Optimum operational conditions for the start-up of helium plasma are found experimentally. Helium and hydrogen plasma operational regimes are discussed, and the extension of the operation domain is proposed for further research.

**Key words:** helium plasma, tokamak, GOLEM, plasma breakdown, operational domain.

## 1. Introduction

Experiments with full helium plasma are quite unique in modern fusion devices. Mostly, these works are made on large scale devices and dedicated to ITER relevant studies for its non-nuclear phase of operation. As it shown, [1] helium plasma performance is always lower than hydrogen or deuterium with identical plasma currents $I_p$, toroidal magnetic field $B_t$, line-averaged core electron densities $\acute{n}_e$ and additional input heating powers. It is shown that in helium tokamak experiments plasma energy confinement time are regularly found to be lower by approximately 30 % compare to the deuterium one. This significantly lower plasma confinement level in real experiments, despite the predictions of gyro-Bohm scaling, is known as isotope effect ( $\rho_{He}=\rho_H$). In order to explain this effect, many theoretical mechanisms are proposed, including $E\times B$ shearing [2] and collisional effects [3]. But still, there is no clear picture of why helium plasmas do exactly have lower overall performance. To collect the necessary information and expand the real experiment data about helium plasma global confinement properties, it will be helpful to investigate its operational domain from small-scale machine point of view, with low values of electron temperature and plasma density.

Current paper is aimed at learning the basics of helium plasma magnetic confinement in small circular-shape fusion device, such as GOLEM. Special attention is paid to the gas breakdown process and its comparison for hydrogen and helium discharges. For this study, a series of discharges with vacuum vessel pre-cleaning have been produced. Hydrogen and helium plasma discharges are studied with identical pre-selected discharge setup parameters allowing one to correctly compare them. Range of plasma parameters that can be achieved on GOLEM are quite modest. Nevertheless mean values of plasma current and line averaged core electron densities for both types of gas are $I_p=2.5-3$ kA, $\acute{n}_e=5\times10^{17}$ m$^{-3}$ respectively. Mean value of toroidal magnetic field during the shot $B_t=0.22$ T.

## 2. The GOLEM tokamak

As it was stated in previous studies [4] the machine itself has a circular cross section with the major/minor radius $R=0.4$ m, $a=0.1$ m. After upgrades the circular stainless-steel vessel is equipped with a molybdenum poloidal limiter of radius $a_l=0.085$ m. Due to the origin of the machine [5] whole vacuum chamber is surrounded by copper shell. The power supply system is fully based on capacitor banks. Each of the individual winding, including central solenoid, is connected to the corresponding capacitor banks, which allows to easily adjust the value of current flowing through the coils to the needs of the experiment. GOLEM's unique capability to be controlled via Internet [6] allows to provide

The machine equipped with set of standard diagnostics [7], which are capable of loop voltage, plasma current, toroidal magnetic field and visible light emission measurements. For dedicated magnetic oscillations plasma studies GOLEM is also equipped with four Mirnov coils. Plasma radiation level is controlled an array of bolometers, hard X-ray (HXR) sensor and a fast camera for time resolved pictures of the visible emission [8,9]. A microwave interferometer ($\lambda=4$ mm) is used for line average electron density measurements. Here we should note that this diagnostic does not operate properly during these experimental series. This fact will be discussed further.

The tokamak operates at maximum toroidal magnetic field of up to 0.5 T, with plasma current less than 8 kA. The central electron temperature is somewhat less than 100 eV, and the line average density just below $1\times10^{19}$ m$^{-3}$, with the maximum pulse length is around 20 ms on hydrogen. GOLEM's gas control system has no options for active gas puffing during the shot. This results in spontaneously core electron density evolution, which will be discussed in next sections.

### 3. Experimental setup

In this work GOLEM was operated remotely by students of the plasma physics department of NRNU MEPhI. Machine operation was performed in so-called "basic mode", when only two capacitor batteries were controlled: one that used for supply of toroidal field coils ($U_{B_t}$) and one that is used to power the primary winding of the iron core transformer ($U_{CD}$). Before the experiment vacuum vessel was carefully conditioned by inductive heating for up to 200 °C for 60 min, which was followed by a cleaning in glow discharge in order to remove impurities adsorbed on the inner surface of the vacuum vessel such as water vapor. Corresponding type of gas for glow discharges were used for H/He type discharges. Standard parameters of the glow discharge cleaning for each type of gas at the GOLEM tokamak are: pressure is around 1 Pa, duration is 20 min., and the discharge current is ~ 0.5 A. Such treatment results in the after overall background pressure around 0.1 mPa.

Due to the gas control system features all experimental data discussed here are performed in typical L-mode scenario with no density control, which is the only scenario that can be implemented on GOLEM now. For easy plasma start-up conditions, in view of difference of the ionization energy for H and He gases, pre-ionization by an electron gun was constantly used. Range of the preselected plasma control parameters for these experiments are presented in the table 1.

| Working gas | $U_{B_t}$ [V] | $B_t$ [T] | $U_{CD}$ [V] | $t_{CD}$ [ms] | p [mPa] | Pre-ionization by electron gun |
|---|---|---|---|---|---|---|
| H/He | 1000 | 0.2-0.3 | 400 - 750 | 0 | 10-230 | ON |

Table. 1. Set of working parameters for the experiment.

Figure 1. Temporal evolution of the plasma column emission measured by the array of bolometers viewing the plasma vertically from the horizontal port (He shot # 30333, center of the vacuum vessel is approximately corresponding to channel no. 10).

Before presenting any experimental results, first it must be noted that the plasma column position in vertical/horizontal direction within the tokamak vessel evolves spontaneously, because it is not actively controlled by feedback. And secondly,

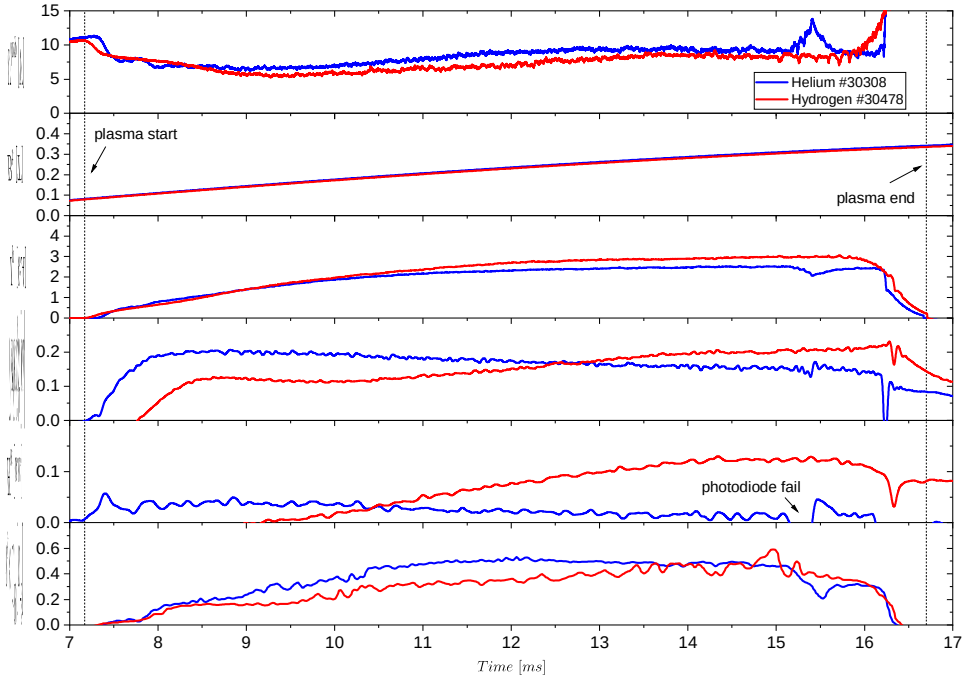


because of the capacitor bank-based system, the value of the toroidal magnetic field is always changing during the plasma discharge. This is a major feature of GOLEM operation at this basic level. Consequently, the plasma column shape and its radius are always evolving during a discharge, as demonstrated in fig. 1 showing typical emission recorded by an array of AXUV bolometers.

With given above discharge set-up parameters it is possible to achieve almost identical shots for both types of prefill gas ( $p_{He,\,prefill}=14$ mPa, $p_{H_2,\,prefill}=16$ mPa). Typical temporal evolution of the main plasma parameters for these H/He discharges are presented in fig. 2.

Figure 2. Temporal evolution of the main plasma parameters for helium (#30308) and hydrogen (#30478) plasma discharges.

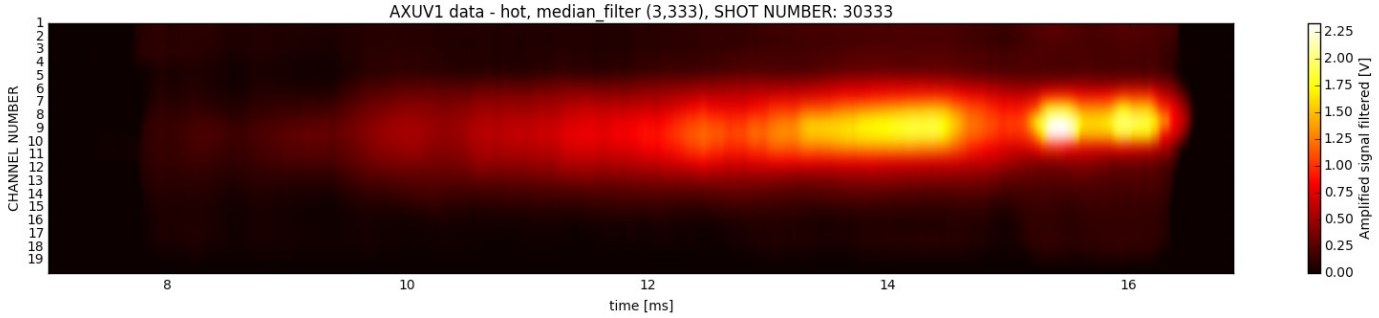


## 4. Experimental results

### 4.1 Breakdown studies

The plasma breakdown is a complex process which involves transition from gas to plasma. After this transition occur, plasma can be confined and controlled by externally supplied magnetic fields and those induced by the current flowing through the plasma itself. The following phase of current rump-up in the presence of a toroidal field requires a constant decrease in resistance and, consequently, an increase in plasma temperature. At its end, the main plasma burn-through phase begins.

Usually breakdown process is described in terms of Townsend avalanche with a given prefill gas pressure $p_{prefill}$, the distance between two electrodes $L$, over which an electric field $E$ is applied [10]. However, it should be noted that this approach is valid when the ionization fraction is small $f_i = 5\%$, and values of electric field is not high ($E_{BD} < 1\,kV$). The electron avalanche would develop if an electron which is accelerated by the electric field, $E_{BD} = 2\pi R$, in case of tokamak, in the gap to sufficiently high energy such that an ionizing collision occurs and a neutral in the gas produces a new electron before it reaches the end of the gap. The first Townsend coefficient, $\alpha$, is the probability of an ionizing collision per unit length times the probability that an electron gains enough energy to ionize neutral:

$$\alpha = \frac{1}{\lambda_{ion}} \exp\left(\frac{-W_{ion}}{E_{ion}}\right) = Ap \exp\left(\frac{-Bp}{E}\right) \quad (4.1)$$

The probability of an ionizing collision per unit length is given by $Ap$, being the inverse of the mean-free-path between ionizing collisions, $\lambda_{ion} = \frac{1}{Ap}$. It is also inversely proportional to the neutral pressure, $p$ , as more collisions are likely for a higher density of gas neutrals. It is important to note that this only concerns ionizing collisions, the mean-free-path between elastic collisions can be much shorter. This fact must be considered, especially for H/He plasma studies. $W_{ion}$, is the energy needed to ionize a neutral, which is in practise higher than the minimum ionization energy, $E_{ion}$. The overall ionization process loses more energy, for example due to some reactions producing in ions being in an excited state resulting characteristic line-emission. $W_{ion}$ value for $H_2$ is typically 20–30 eV and for He is in range of 70-80 eV. The parameters $A$ and $B$ depend on $W_{ion}$ and $\lambda_{ion}$and thus the ionization cross-section $\lambda = \frac{1}{n\sigma}$.

Solving equation (4.1) for case of long gaps, when $\alpha L > 1$, gives: $E_{BD} = \frac{Bp}{\ln(ApL)}$ , where $L$ – is connection length, the length of the magnetic field line trajectory along which the electrons could travel. This relationship leads to existence of the minimal value of breakdown electric field, which is connected to so-called Stoletov's constant point, where $\bar{e}\frac{B}{A} = \bar{e}\frac{W_{ion}}{e}$. Value at this point correspond to the minimum breakdown voltage needed to sustain a Townsend avalanche. By assuming that the value of connection length should not change significantly for different types of gas, it is possible to estimate the constants $A$ and $B$, from approximation of the experimental data.

Figure 3 shows the experimental curves obtained by multiple parameter fitting for the H/He data. It's clear that helium operation domain is in range of higher electric fields for the same values of $p \times L$, as $E_{ion,He}$ is higher. The best fit was achieved with values of $A = 3.8\,Pa^{-1}m^{-1}$, $B = 96\,V\,m^{-1}\,Pa^{-1}$ for hydrogen, and $A = 3.2\,Pa^{-1}m^{-1}$, $B = 260\,V\,m^{-1}\,Pa^{-1}$, for helium. It must be noted that the values are a rough approximation and should be treated carefully. Nevertheless, these values are lower than table values for corresponding gases, due to the additional source of electrons which are supplied by the electron gun. This results in lower expected values of needed minimum energy to ionize the neutral $W_{ion,H} = 52\,eV$, $W_{ion,He} = 82eV$?

Figure 3. The Pashen's curve fitting for helium and hydrogen plasma discharges.

### 4.2 Start-up evolution of the helium discharge (low vs high $p_{prefill}$)

Figure 4. Temporal evolution of the start-up phase of typical helium vs hydrogen plasma parameters that were implemented in these experimental series.

Next step is estimation of the initial gas pressure dependence on overall plasma performance. For this purpose, two discharges with almost twice difference in gas pressure were selected. Both have similar toroidal magnetic field evolution and pre-selected discharge parameters values. With increase of the working gas pressure level it is expected to decrease of the mean free

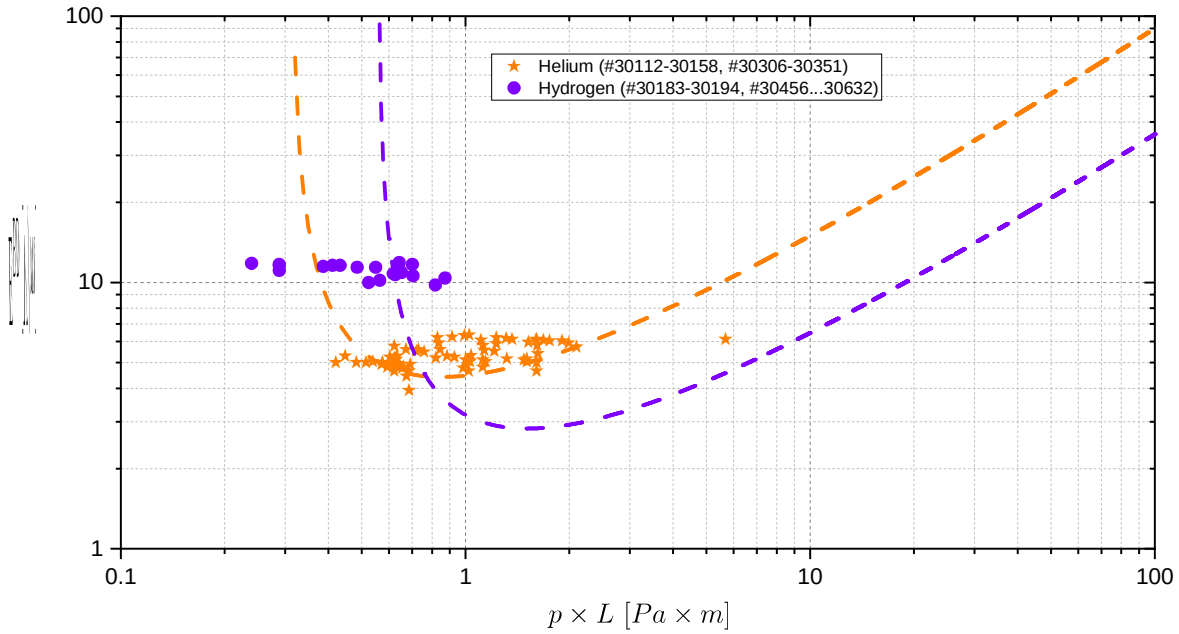


path distance value, which results in lower breakdown loop voltage and toroidal magnetic field levels. This fact is shown in fig. 4, in the same way electron avalanche time is also lower in case of higher gas pressure. In final there is significant rise in discharge length from 9.7 to 10.6 ms.

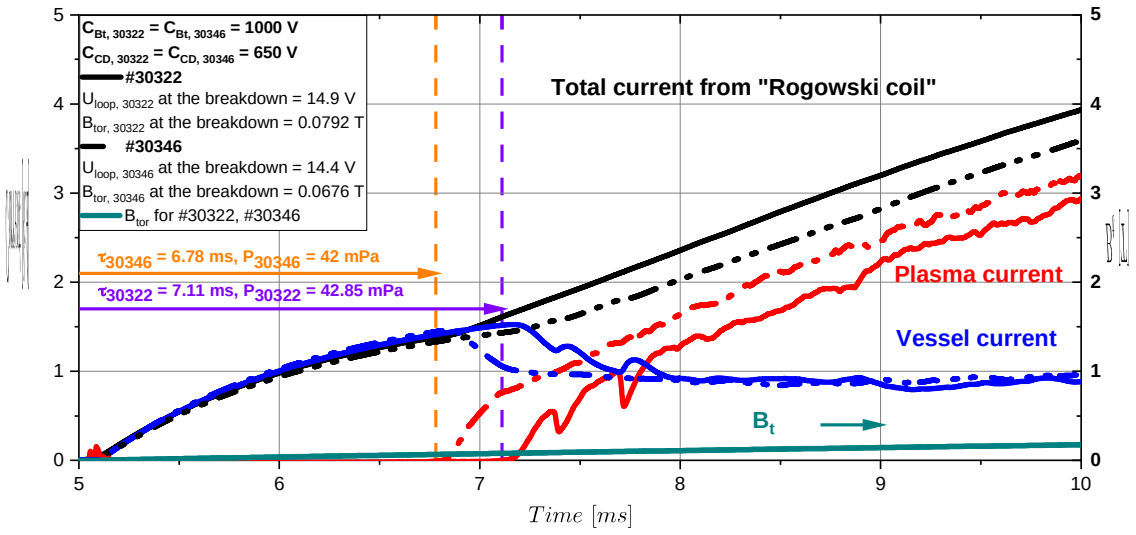


### 4.3 Macroscopic plasma parameters

During experiments dependency of the maximum plasma current $I_{pl_{max}}$ on $U_{CD}$ and the gas pressure was measured:

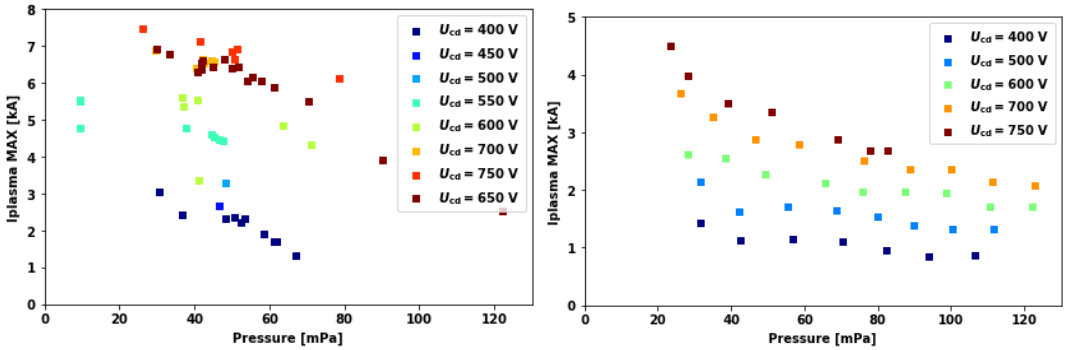


Figure 5. Dependency of $I_{pl}$ max. on $U_{CD}$ and pressure. On the left hydrogen plasma, on the right helium plasma

Dependency of breakdown voltage on $U_{CD}$ and gas pressure:

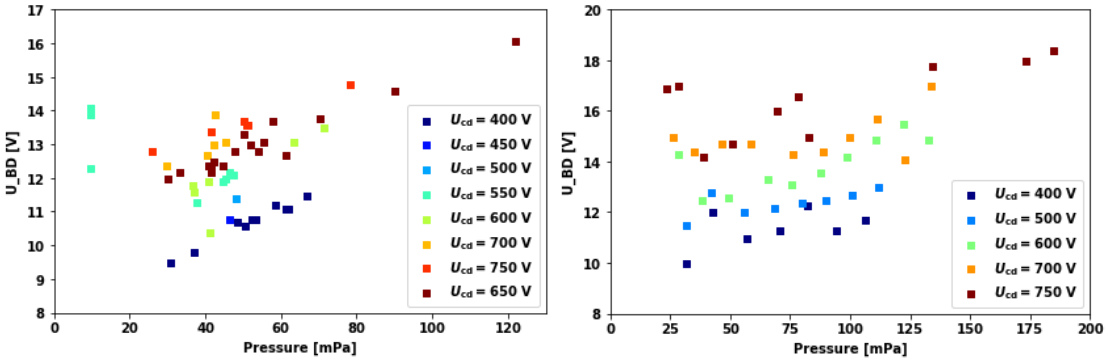


Figure 6. Dependency of $U_{BD}$ (breakdown voltage) on $U_{CD}$ and pressure. Left panel - hydrogen plasma, right - helium plasma

It is interesting to note that the breakdown voltage in hydrogen plasmas is almost independent on $U_{CD}$, but proportional

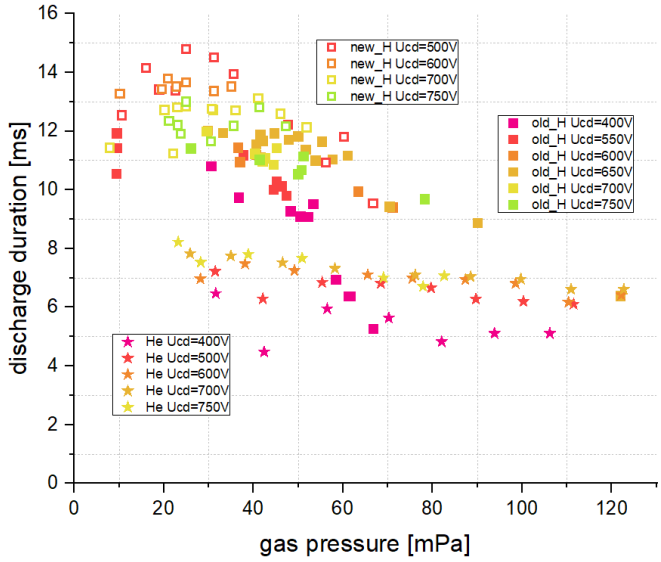


to the pressure of the working gas. Opposite behavior is observed in helium plasmas.

Figure 7. Dependences of the duration of the plasma discharge on the pressure of the working gas

Dependences of the duration of the plasma discharge on the pressure of the working gas in the chamber before shots for different current-drive voltages were plotted (fig. 7). The presence of instabilities for most hydrogen discharges, which are manifested in drops in the plasma current level, their duration has a more random distribution, not only because of the effect of these instabilities on the discharge, but also because of the difficulty in determining the duration of the discharge. Nevertheless, using the example of hydrogen shots, it can be seen that the discharge duration depends on the state of the tokamak chamber:

1. Discharge durations for the first hydrogen series have lower values than the durations of the second hydrogen series;

2. For the second hydrogen series higher current-drive voltages correspond to the higher discharge durations, however, this is not very evident for the first hydrogen series.

Helium discharges are less susceptible to the development of such instabilities. For this discharges the dependence of the duration of the discharge on the gas pressure in the chamber is close to linear.

First type of instabilities is presented here. This instability is characteristic of hydrogen discharges at a sufficiently high gas pressure in the chamber compared to those used in the series. During discharges with such parameters, a single drop in the plasma current is observed at the end of the discharge, but it does not lead to a direct disruption of the plasma. It is worth noting the weak dependence in the development of this instability on current-drive voltage.

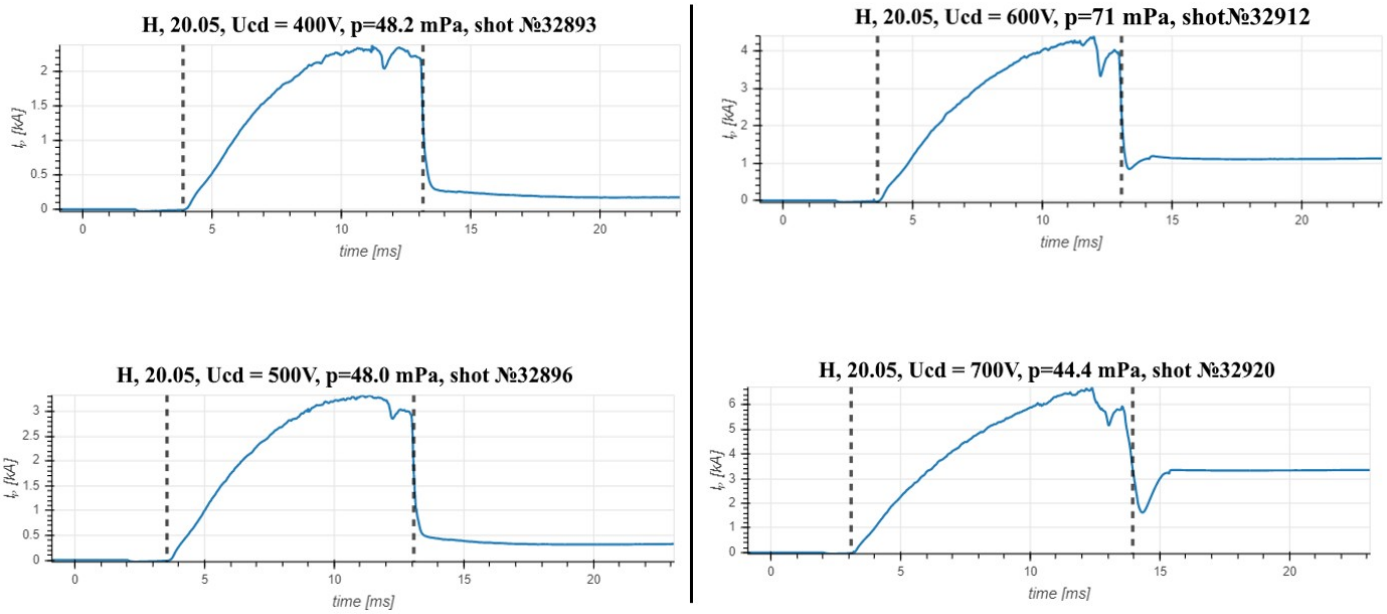


Figure 8. Presence of some instability for H-discharges

Here it is possible to determine the value of the safety factor on the edge of plasma q(a) at the time this instability occurs. Due to an increase in the plasma current and compression of the plasma column due to a displacement of its axis, the safety factor drops below 2, that leads to the development of MHD instability. For helium discharges, such instabilities are observed only in isolated cases, like other instabilities, which will be described later.

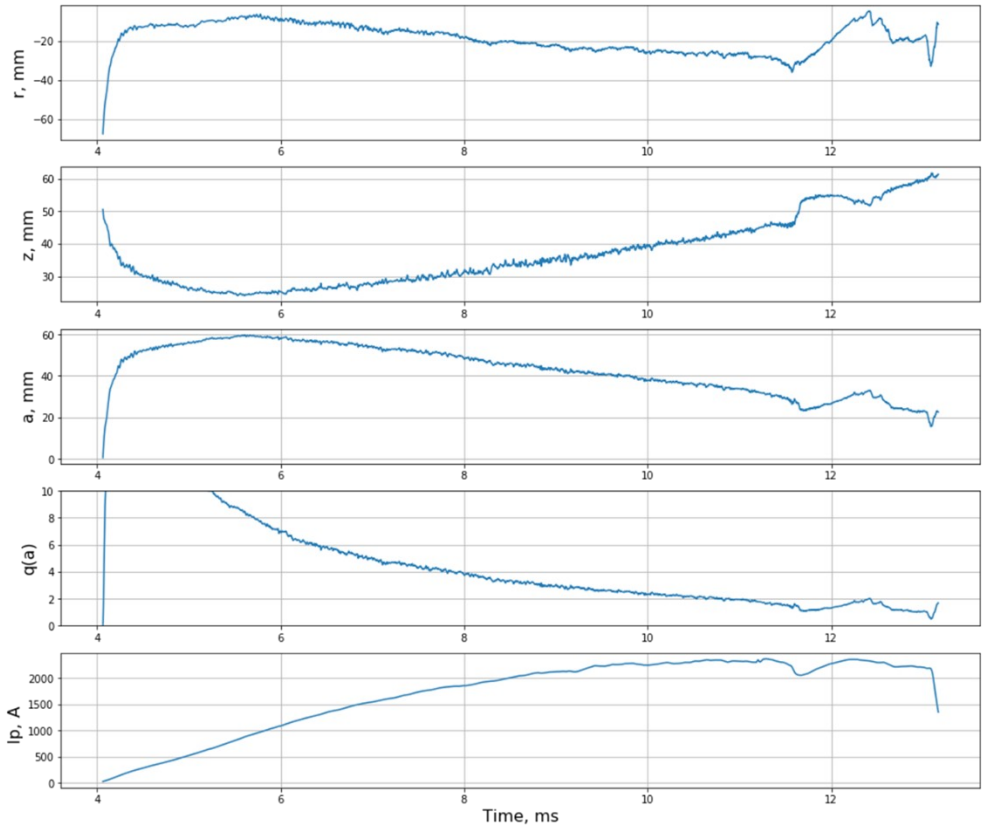


Figure 9. Occurring of instability when safety factor drops below q(a) = 2

For hydrogen discharges, the minimum value of the q(a) is limited to 2, which suggests that sawtooth oscillations are observed, although similar instabilities develop even with large values of the q(a).

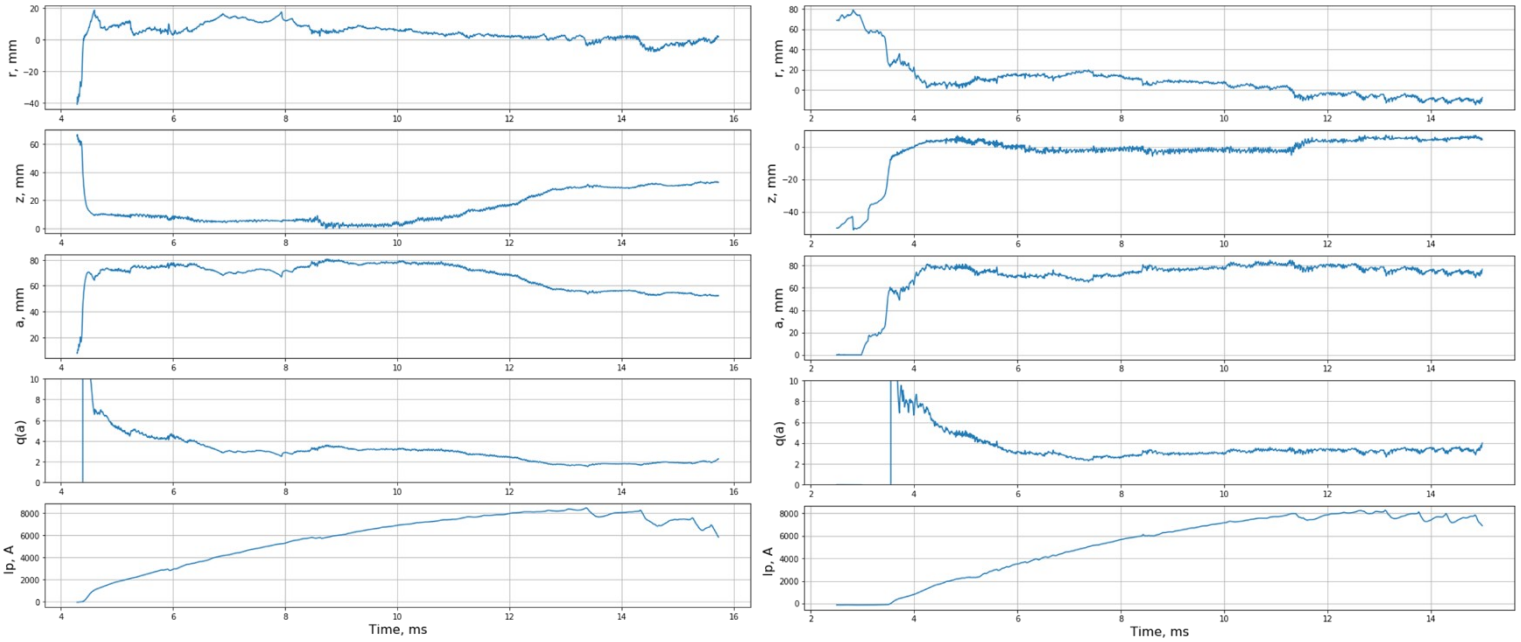


Figure 10. Occurring of instability when safety factor drops below 2 (left pic.) or above 2 (right pic.)

### 4.4 Plasma shifting

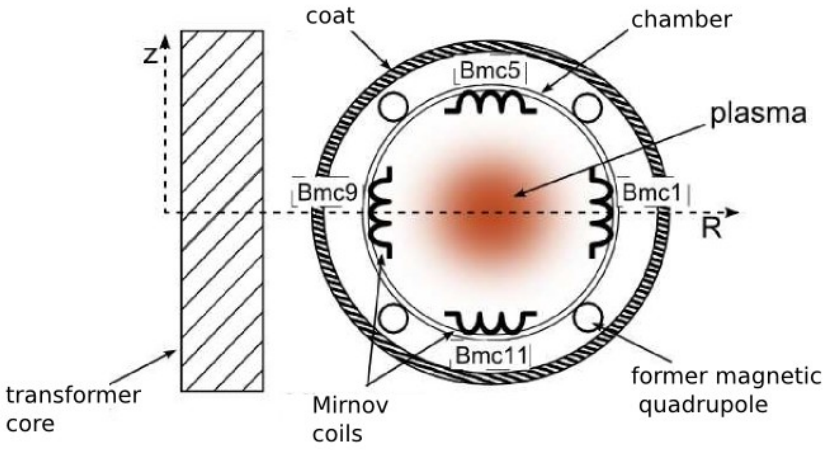


Figure 11. Locations of Mirnov coils

Mirnov coils are from magnetic diagnostic family and are used to the plasma position determination on GOLEM. 4 Mirnov coils are placed inside the tokamak 93 mm from the center of the chamber and their locations are depicted in fig. 11. The effective area of each coil is $A_{eff} = 3,8 \cdot 10^{-3}\, m^2$. Coils mc9 and mc1 are used to determination the horizontal plasma position and coils mc5 and mc13 to determination the vertical plasma position.

The coils measure voltage induced by changes in poloidal magnetic field. In order to obtain measured quantity (poloidal magnetic field), it is necessary to integrate the measured voltage and multiply by constant:

$$B(t) = \frac{-1}{A_{eff}} \int_0^t U_{sig}(\tau)\, d\tau$$

Ideally axis of the coils is perpendicular to the toroidal magnetic field, but in fact they are slightly deflected and measure toroidal magnetic field too. For determination plasma position this additional signal should be eliminated. Vacuum discharge with same parameters as plasma discharge is used for these purposes. The signal that measure Mirnov coils during the vacuum discharge includes signal from toroidal magnetic field and usually also from some other magnetic field e.g. generated by windings. This signal is subtracted from the active signal during plasma discharge.

Straight conductor approximation is made for calculation of plasma column displacement. With values of poloidal field on the two opposite sides of the column, its displacement can be expressed as: $\Delta = \frac{B_{\theta=0} - B_{\theta=\pi}}{B_{\theta=0} + B_{\theta=\pi}} \cdot b$ , where 2b is the distance between measuring places (2×93mm).

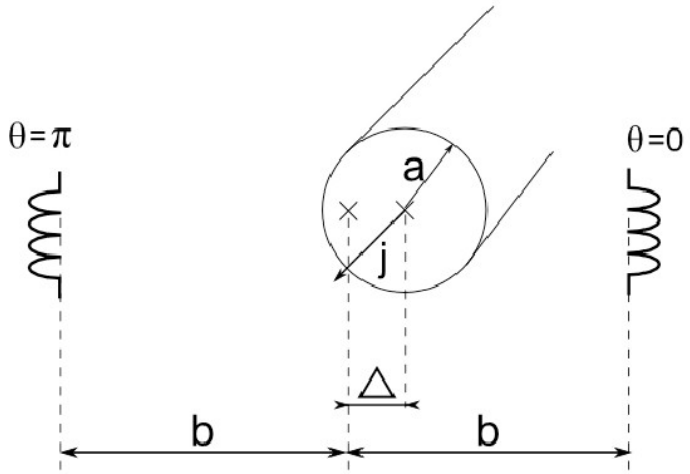


Figure 12. Schematic picture for plasma displacement calculation

Specifically, for determination horizontal plasma displacement:

$$\Delta r = \frac{B_{mc1} - B_{mc9}}{B_{mc1} + B_{mc9}} \cdot b$$

and for vertical plasma displacement:

$$\Delta z = \frac{B_{mc13} - B_{mc5}}{B_{mc13} + B_{mc5}} \cdot b$$

if Δr and Δz are known, plasma column radius *a* can be calculated too:

$$a = a_0 - \sqrt{\Delta r^2 + \Delta z^2}$$

where $a_0 = 85\,mm$ (position of limiter).

The radius displacement is less than zero, which means that plasma column is forced to held more inward position. This is on the contrary with the usual picture, when $\Delta r > 0$. The reason of such behavior can lie in some windings of the GOLEM tokamak which give rise of additional attractive inward-directed forces.

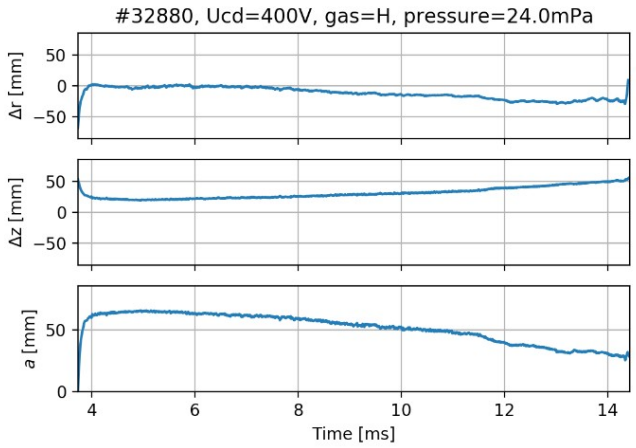


Figure 13. Plasma position time dependencies.

Characteristic point of time should be chosen where we measure displacements as dependencies similar to what is shown on fig.13 were calculated for almost all shots and such dependencies are hard to compare. It was decided to take the maximum current moment time as such point. $\Delta r$ , $\Delta z$ , $a$ were averaged on 20 time points (1μs distance between points) around plasma current peak.

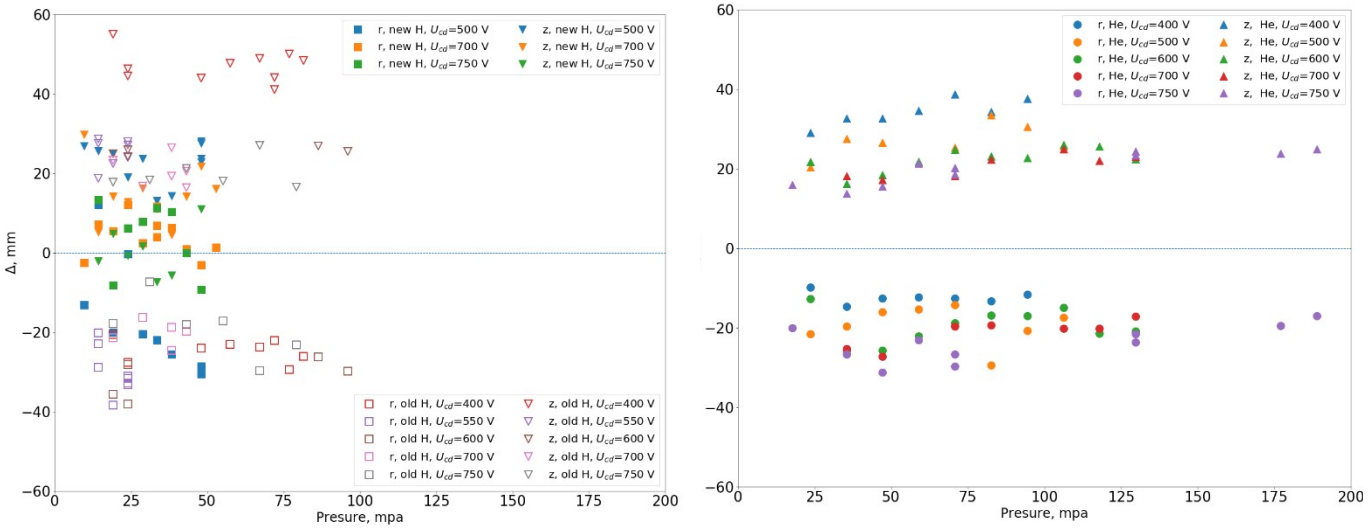


Figure 14. Pressure scans for plasma position are shown on figures 4 (hydrogen shots) and 5 (helium shots)

$U_{CD}$ mentioned on the figures is current drive voltage which is connected with plasma current value. It is clearly seen that there is almost no dependency on pressure for all helium sets. Plasma column was always located inwards and upwards in the vessel. The figure with hydrogen sets is quite messy but again no pressure dependency is seen. However, the position of “new” hydrogen shots is more central comparing with both “old” hydrogen and helium shots.

It should be mentioned that ‘new H’ shots were made after lots of helium shots. It is known that plasma behavior strongly depends on vacuum chamber preparation procedure. So, such change in parameters can be attributed to better chamber conditioning (chamber is somewhat cleaner due to walls degassing by discharges).

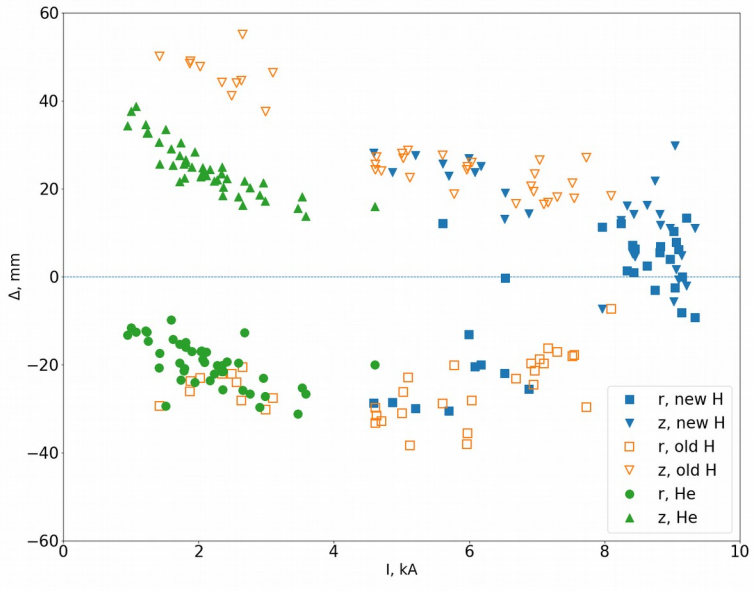


Figure 15. Plasma current scan

Plasma current position became more downward and inward shifted for helium shots, which is not the case for hydrogen shots. A tendency for locating more central is common for both sets of hydrogen shots. Also we can see that plasma currents for “new H” are larger than for both “old H” and helium which also can be attributed to cleaner vacuum chamber.

### 4.5 Plasma fluctuations

Fast Fourier Transform (FFT) technique was used to plot spectrograms of received signals from magnetic coils. Let $F_1(f), F_2(f)$ denote the respective Fourier transforms. The resultant cross-spectrum is computed from: $P_{12}(f)=F_1^{¿}(f)F_2(f)$, where the asterisk denotes a complex conjugate. In general, $P_{12}(f)$ is complex, so it may be presented as follows:

$$P_{12}(f)=\left|P_{12}(f)\right| e^{i\phi_{12}(f)}$$

where $\left|P_{12}(f)\right|$ is absolute value of cross-spectrum and $\phi_{12}(f)$ is cross-phase of two signals.

That way, the cross-phase of signals from Mirnov coils can be calculated from real and imaginary parts of cross-spectrum elements. Another useful function that can be calculated from cross-spectrum is coherence of two signals. The coherence values is determined as follows [11]:

$$C_{12}(f)=¿P_{12}(f)\vee \frac{¿}{\left[P_{11}(f)P_{22}(f)\right]^{1/2}}¿$$

The example of FFT spectrograms is shown in Figure 2. The figure also presents time dependencies of plasma current and loop voltage during discharge. Each spectrogram is related to one of Mirnov coils. Time-averaged power spectral density (PSD) is shown under each spectrogram. All the graphs are bounded in time by the start and end of plasma discharge. One can see that after 12 ms some oscillations appear in plasma current. Additionally, some coherent fluctuations of magnetic field appear at $f\sim 25\,kHz$ as it can be seen in spectrograms.

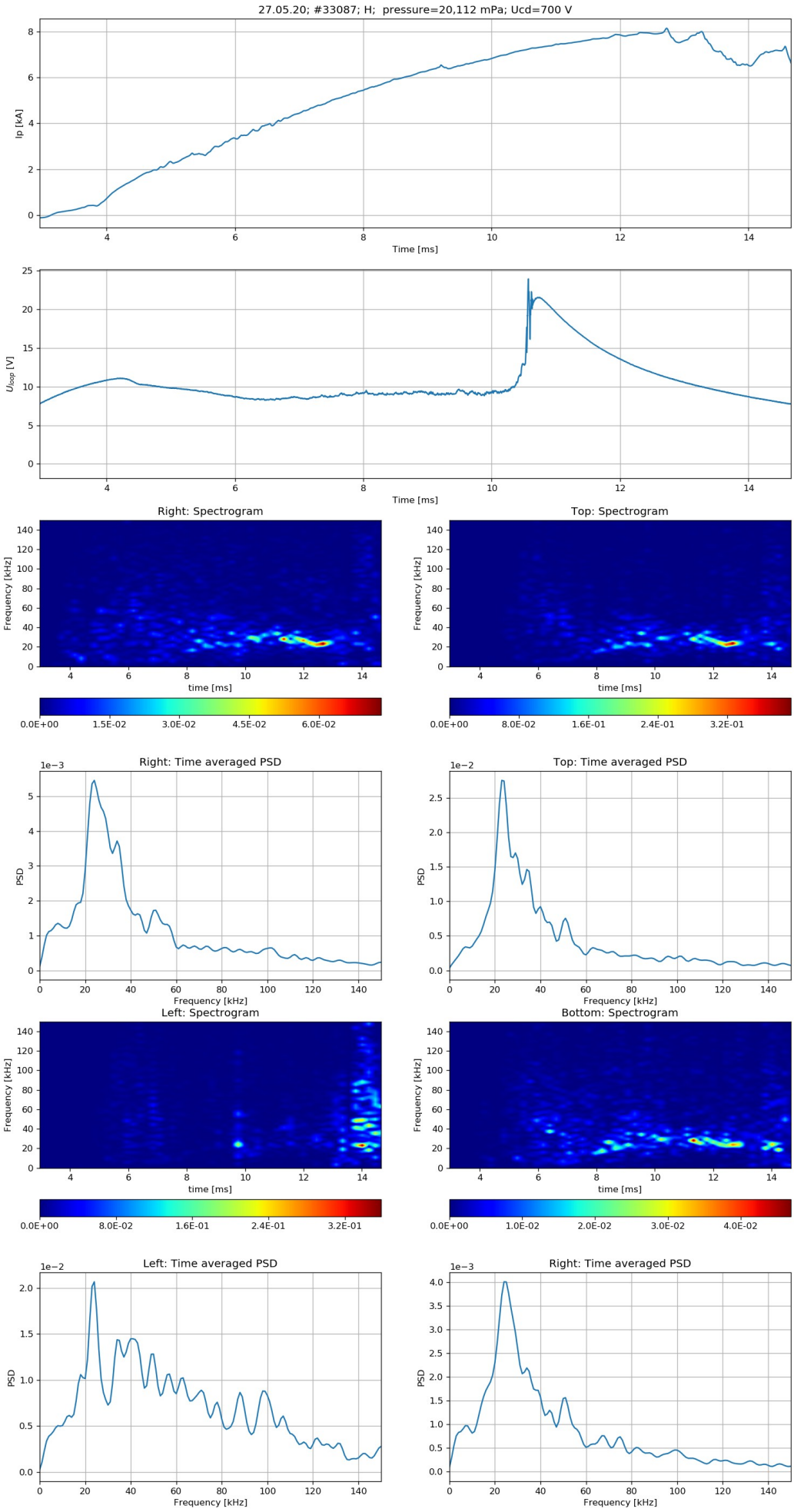


Figure 16. Spectrograms of shot #33087. Colormap represents power spectral density

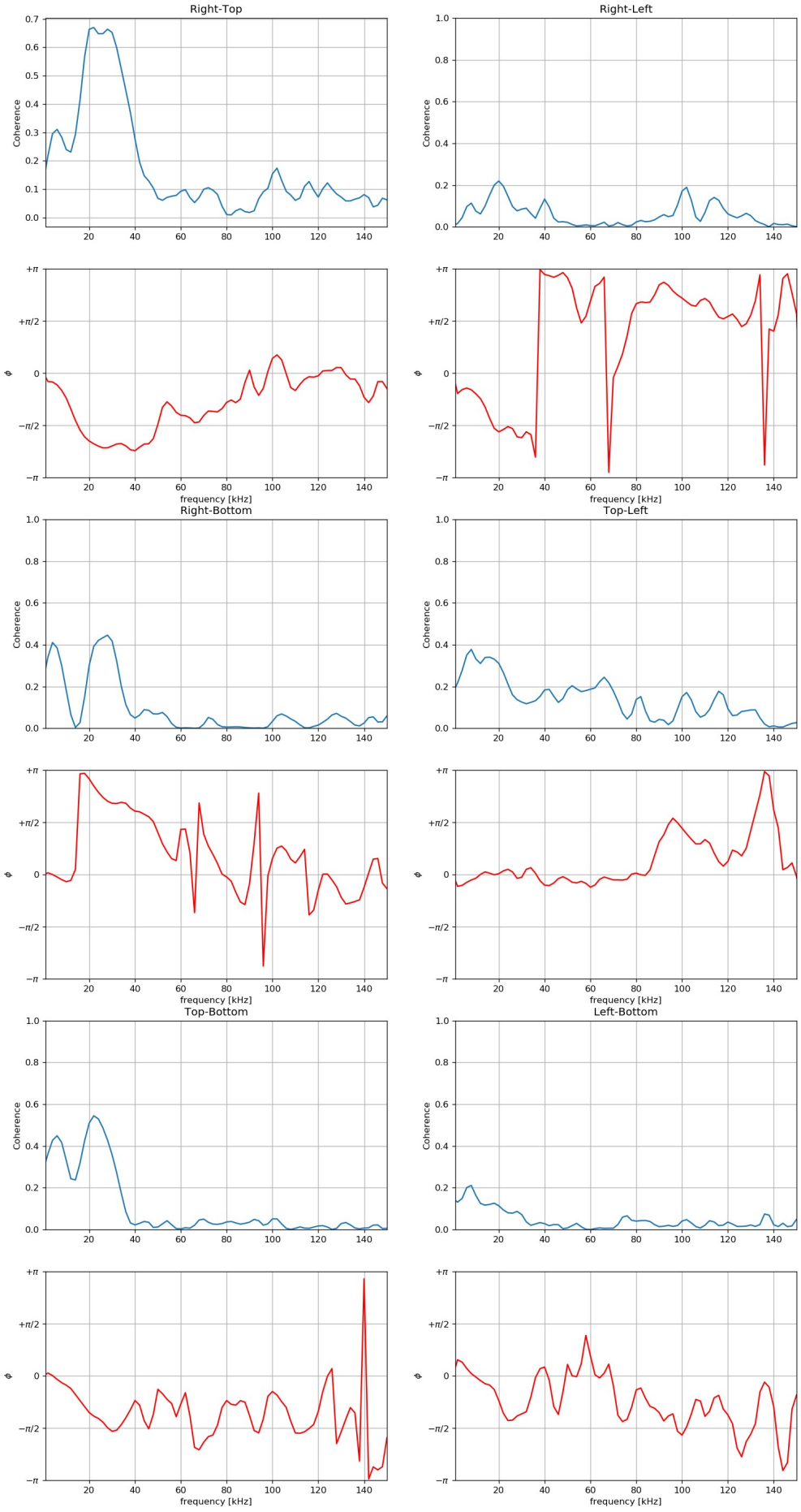


Figure 17. Cross-coherence and cross-phase for shot #33087

However, left coil does not reproduce such fluctuations, but, probably, shows some turbulence at the end of discharge. (That could be caused by the plasma shift in horizontal direction?). Time-averaged PSD have clear peaks at $f \sim 25\,kHz$. Further

analysis can be provided by cross-coherence and cross-phase analysis. These dependencies are shown in Figure 3. The left series of graphs show some correlation at $f \sim 25\,kHz$. That way, the phase shift between two coils can be estimated. He-shots does not show any coherent fluctuations. An example of spectrogram for He-discharge is shown in Figure 4. Probably, these spectrograms shows the appearance of some turbulence at the end of the discharge.

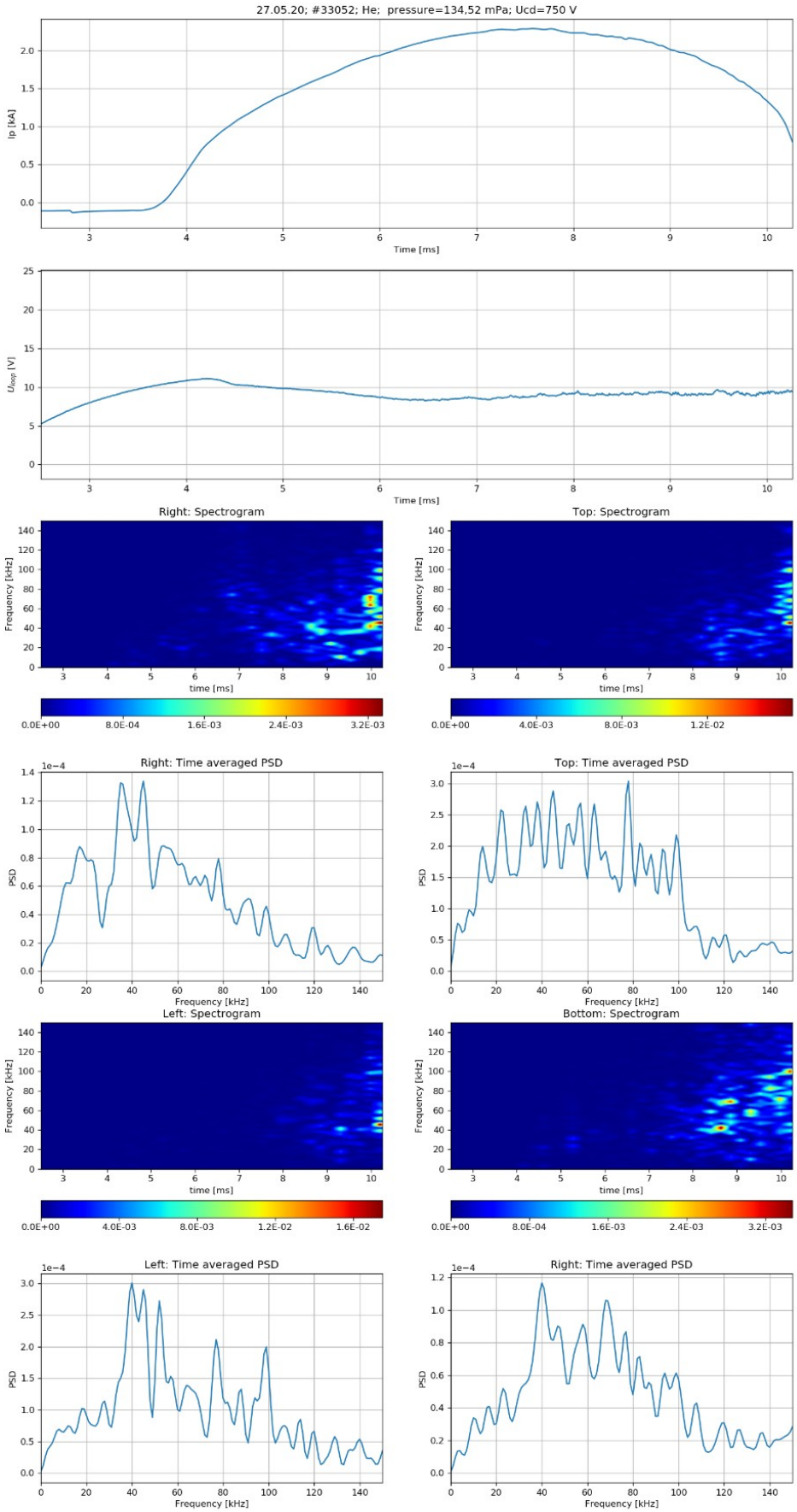


Figure 18. Spectrograms of shot #33052. Colormap represents power spectral density

### 4.6 Electron temperature estimation

In order to measure the electron temperature at the edge of plasma several probes were used. The measurement technique is presented in the fig.19,20. Ball-pen probe is used to measure the plasma potential. Langmuir probe measures floating potential. [12] Also, there is double tunnel probe in the plasma. First tunnel probe is directed along the plasma current toward the limiter, so it was marked as Lim. The second tunnel probe is pointing in the opposite direction and it was called OLim. The tunnel probes are used to measure the floating potential, too.


Fig 19: Photos of probes on GOLEM tokamak. On the left – Ball-Pen and Langmuir probe, on the right – double tunnel probe

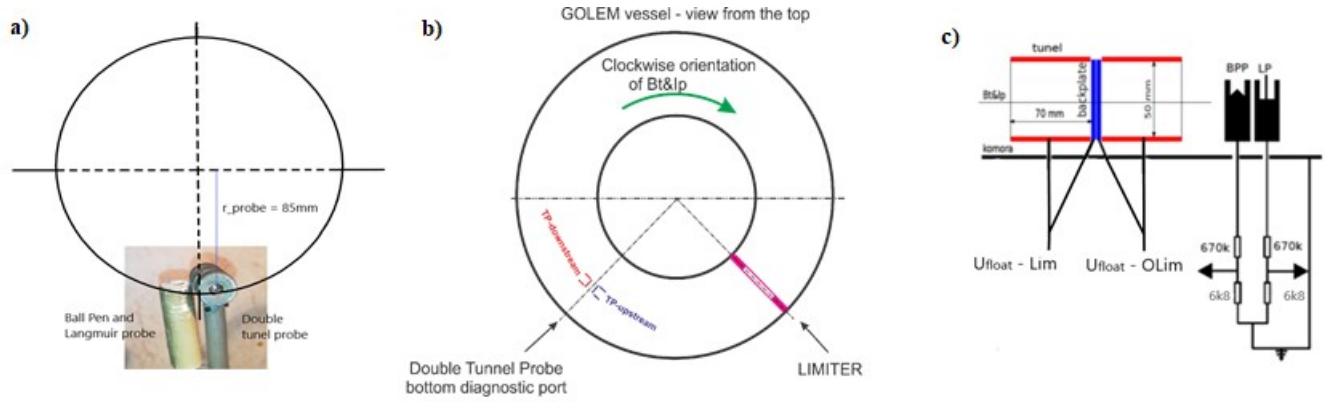


Figure 20 (a) Poloidal cross section with placed Ball-pen and Langmuir probes. (b) Top view with placed double tunnel probe. (c) Electrical circuit of the probes.

To find the electron temperature in the plasma the expression was used:

$$T_e = \frac{\varphi - U_{float}}{\alpha}$$

Here $T_e$ is the electron temperature in the eV units; $\varphi$ is the plasma potential, measured with Ball-pen probe; $U_{float}$ is a floating potential, which can be measured with one of the three probes left; both $T_e$ and $U_{float}$ have been measured in V units;$\alpha$ is a calibration factor, which is equal to 2.5 for $H_2$ discharges and 2 for He discharges. The graphs, presented in the Figure 21, demonstrate dependencies of electron temperature at the moment of maximum plasma current on parameters of the discharge.

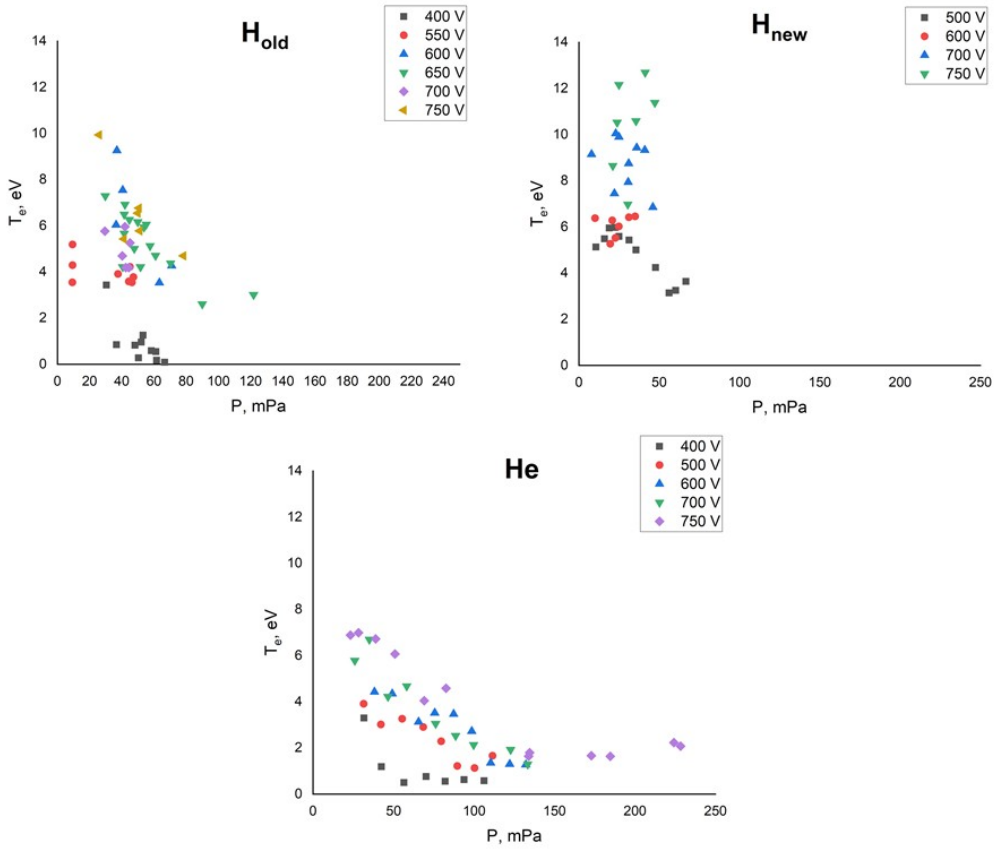


Figure 21. Electron temperature dependencies on initial gas pressure and current drive voltage at the moment of maximum plasma current. Indices “old” and “new” denotes the experiments with hydrogen provided on different days.

The graphs in Figure 2 show that electron temperature tends to reduce when pressure value is increasing. Current drive voltage, which is supplying the central solenoid, was found to increase the electron temperature value. The other effect observed is that at the increasing of the current drive voltage the electron temperature dependence on pressure becomes more abrupt. The fact that helium is heavier than hydrogen by a factor of four leads to more radiative losses from the plasma. This explains, that for He discharges electron temperature became lower, than for H discharges. The current drive voltage must directly influence the plasma current value. Since GOLEM has only Ohmic heating, the current increasing leads to increasing of the electron temperature. This tendency is shown in the fig. 22.

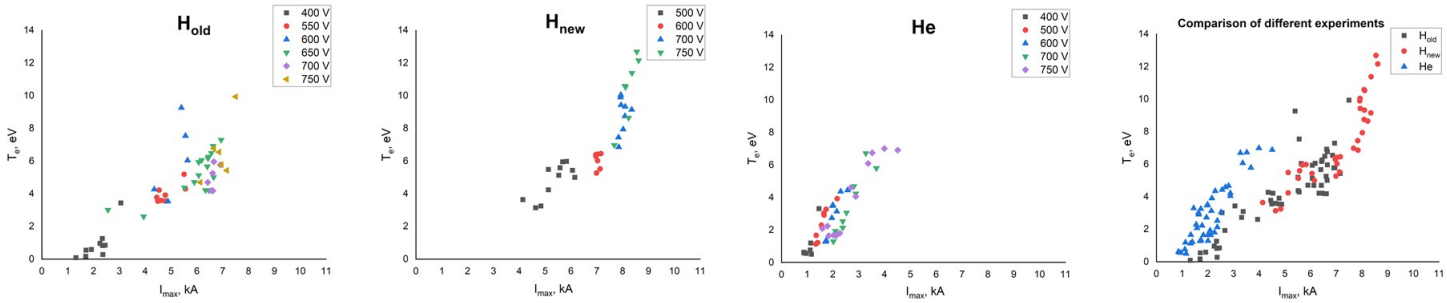


Figure 22. Electron temperature dependencies on maximum plasma current among the discharge for different values of current drive voltage. The electron temperature values were chosen at the moment of maximum plasma current.

As one can see from fig. 22, both the plasma current and current drive voltage contribute to increase electron temperature. As was mentioned, the He temperature is lower for the same values of plasma and current drive voltage. Bottom right graph presents combined three other graphs without any information about current drive voltage. The spectrograms for different discharges were built to see the frequency spectrum and time evolution of the probes signal. The typical spectrograms for H and He discharges are presented in fig. 23.

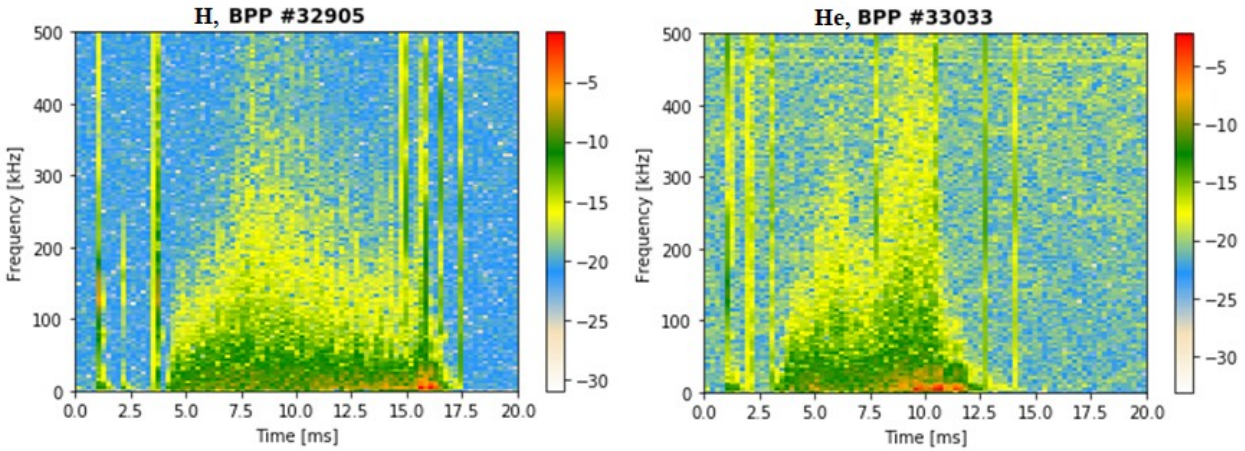


Figure 23. Typical spectrograms of Ball-Pen Probe signal for H and He discharges. The colorbar shows values of the logarithm of power spectral density.

The discharge time for He was found to be lower, than for H. At the end of all the discharges the contribution of low frequencies is increasing. The increasing of current drive voltage leads to more contribution to the power spectral density through all frequency range. At the same time the lower pressure value insignificantly stabilizes some perturbations.

For central electron temperature estimation was used equation:

$$T_e(0) = \left( \frac{8R}{a^2 \cdot 1.544 \cdot 10^3} \right)^{2/3} \left( \frac{Z_{eff} I_{pl}}{U_{loop}} \right)^{2/3}$$

where major radius R = 0.4 m, a is minor radius and $Z_{eff}$ is effective ion charge.

For helium $Z_{eff}$ = 4 , so $T_e(0)=4.1\cdot\left(\frac{I_{pl}}{a^2 U_{loop}}\right)^{2/3}$ and for hydrogen with $Z_{eff}=2{,}5$ $T_e(0)=3\cdot\left(\frac{I_{pl}}{a^2 U_{loop}}\right)^{2/3}$ .

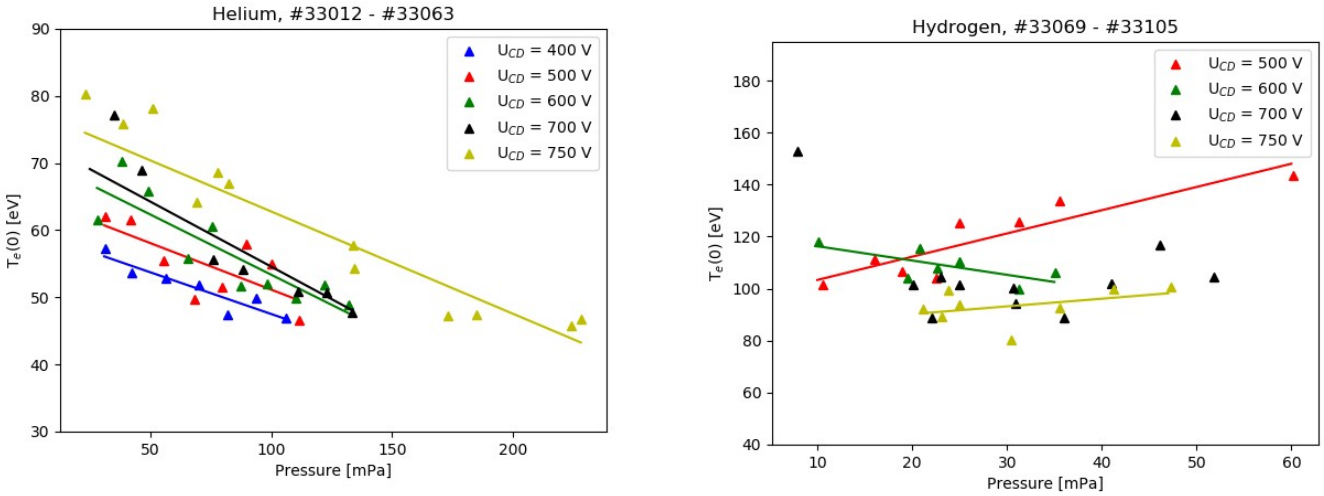


Calculations for held experiment are presented in fig. 24.

Figure 24. Dependence of central electron temperature from current drive voltage.

Thereby global energy confinement for electron component could be calculated. We can try to calculate average electron density:

$$\tau_e=\frac{2}{3}\frac{p}{T_{ch}}\frac{T_e(0)\cdot V}{U_{loop}\cdot I_{plasma}}[ms;m^{-3},K,m^3,V,A,Pa]$$

where plasma volume $V = 2\pi^2 \cdot R_o \cdot a^2$ , and $a$ is actual minor radius and $\acute{n}_e = \frac{2p}{k_B \cdot T_{ch}}$ – avarage electron density. As it could be seen on figure 10, for helium shots were observed that $\tau$e increase proportionally with pressure and inversely with $U_{CD}$ for

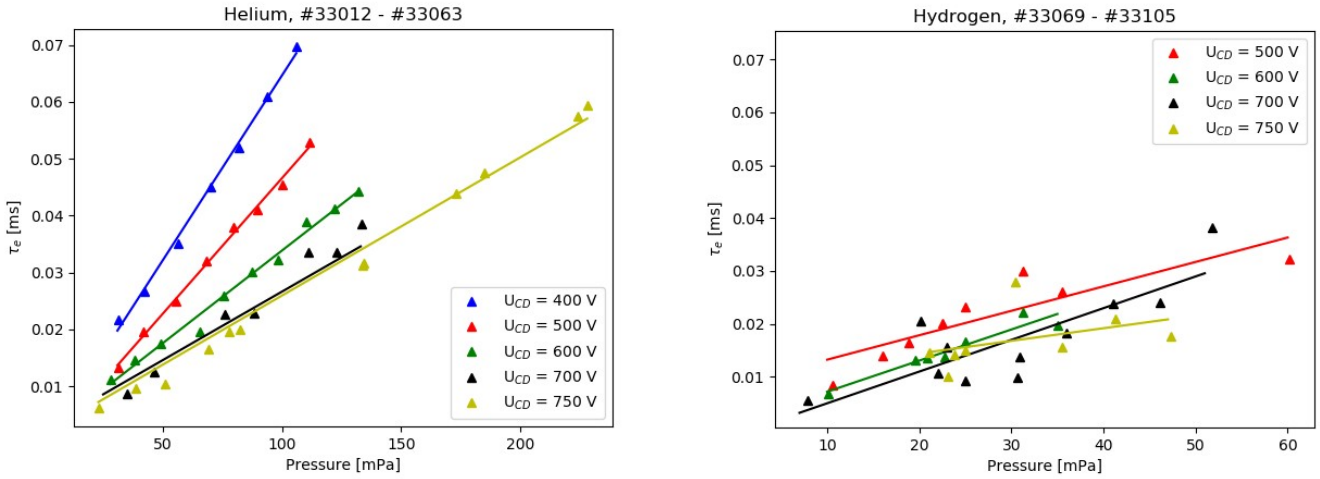


hydrogen shots dependencies were not clear.

Figure 25. Dependence of global energy confinement for electron component from gas pressure.

## 5. Conclusion

For summarizing whole experiment's results, we can highlight general trends. Helium shots are about 1 – 2 ms shorter than the hydrogen ones. Electron temperatures in helium are dependent on current drive and pressure – with increasing $U_{CD}$, the electron temperature is also increasing and with increasing pressure, the electron temperature is decreasing. For helium shots were observed that $\tau_e$ increase proportionally with pressure and inversely with $U_{CD}$ and for hydrogen shots dependencies were not clear. It was shown that for most of shots plasma was shifted inward that is not usual for tokamaks. Also, it was shown that there was almost no dependency on initial gas pressure. However, difference in behavior of 'new H' and 'old H' was clearly seen. 'new H' shots were more central. It can be explained with the fact that 'new H' shots were held after helium shots and vacuum chamber could be somewhat cleaner than for other sets. Moreover, maximum plasma currents for these shots were higher, which can be attributed to the same reason. As for plasma current scan, difference in behavior between helium and hydrogen shots was mentioned. Plasma was less shifted with increasing maximum plasma current for hydrogen shots. As for helium, plasma column became more inward and downward shifted for plasma current increasing.

## 6. References


[1]. The confinement of helium tokamak plasmas, impact of electron heating, turbulent transport and zonal flows. https://iopscience.iop.org/article/10.1088/1741-4326/aaeeb5/pdf
[2]. Waltz R.E., Dewar R.L. and Garbet X. 1998 Phys. Plasmas 5 1784
[3]. Nakata M., Nunami M. and Sugama H. 2017 Phys. Rev. Lett.118 165002
[4]. Operational Domain in Hydrogen Plasmas on the GOLEM Tokamak
[5]. Remote operation of the GOLEM tokamak with hydrogen and helium plasmas
[6]. V. Svoboda, B. Huang, J. Mlynar, G.I. Pokol, J. Stöckel, G. Vondrasek, Multi-mode remote participation on the GOLEM tokamak. Fusion Eng. Des. 86, 1310–1314 (2011)
[7]. I.H.Hutchinson, Principles of plasma diagnostics, doi: 10.1017/CBO9780511613630
[8]. Low cost alternative of high speed visible light camera for tokamak experiments
[9]. Progress in application of high temperature superconductor in tokamak magnets
[10]. A. Von Engel, Ionized gases, 1965
[11]. E. J. Powers and G. S. Caldwell, "Fast-fourier-transform spectral-analysis techniques as a plasma fluctuation diagnostic tool," IEEE Trans. Plasma Sci., 1974.
[12]. R. Dejarnac, J.P. Gunn, J. Stockel, J. Adamek, J. Brotankova, C. Ionita, Study of ion sheath expansion and anisotropy of the electron parallel energy distributionin the CASTOR tokamak, Plasma Physics and Controlled Fusion 49, 1791-1808 (2007).